Journal of Theoretical and Applied Information Technology
15th March 2021. Vol.99. No 5

ISSN: 1992-8645 www.jatit.org E-ISSN: 1817-3195

STATISTICAL FEATURE LEARNING THROUGH ENHANCED DELAUNAY CLUSTERING AND ENSEMBLE CLASSIFIERS FOR SKIN LESION SEGMENTATION AND CLASSIFICATION

ADIL H. KHAN[1,2], D.N.F. AWANG ISKANDAR[1], JAWAD F. AL-ASAD[2], SAMIR EL-NAKLA[2], SADIQ A ALHUWAIDI[2]

[1]Faculty of Computer Science and Information Technology, Universiti Malaysia Sarawak, Malaysia

[2]Department of Electrical Engineering, Prince Mohammad Bin Fahd University (PMU), Saudi Arabia

E-mail: [2]akhan@pmu.edu.sa, [1]dnfaiz@unimas.my, [2]jalasad@pmu.edu.sa, [2]snakla@pmu.edu.sa, [2]salhuwaidi@pmu.edu.sa

ABSTRACT

There are multiple types of skin cancer but melanoma is the deadliest skin cancer or lesion type. Early recognition of melanoma in dermoscopy images essentially increase the endurance rate. However, the precise acknowledgment of melanoma is very challenging because of the numerous reasons: low difference among lesion and skin, visual comparability among melanoma and non-melanoma lesions, and so forth. Consequently, the dependable programmed diagnosis of skin cancer is exceptionally helpful to dermatologist. In this paper, we proposed profound learning strategy to address three primary assignments developing in the zone of skin lesion picture preparation, i.e., dermoscopic highlight, extraction and detection. A profound algorithm comprising of preprocessing in CIELAB color space and Delaunay triangulation based clustering along with Particle Swarm Optimization (PSO) is proposed for the segmentation. Moreover, skin lesion images are clustered based on fused color, pattern and shape based features. A boost ensemble learning algorithm using Support Vector Machines (SVM) as initial classifiers and Artificial Neural Networks (ANN) as a final classifier is employed to learn the patterns of different skin lesion class features. The proposed automated system is assessed on the ISIC and PH2 datasets. Test results show the promising efficiency of our proposed study, i.e., 96.8% and 92.1% segmentation accuracy for ISIC and PH2 datasets respectively. Classification accuracy of 97.9% also accomplished on ISIC dataset. It can be concluded from this research that proposed system employed the power of simple methods that are less resource-hungry yet provide better results.

Keywords: *Skin Lesion, Artifacts Removal, Delaunay Triangulation, Features Fusion, Ensemble Classification*

1. INTRODUCTION

Melanoma is the most malignant and deadliest type of skin cancer or lesion and the death rate due to this is increasing all over the world. As per statistical data provided by American cancer society in 2019 almost 91,000 people all over the world are diagnosed with skin cancer type melanoma out of which more than 7,000 people die due to this disease [1]. These cases of skin cancer are mainly associated with ozone layer degradation and tanning [2]. But this disease can easily be cured if detected early by a simple surgery of excision and the patient can lead to normal life later [3]. In general skin cancer is divided into two main categories, Benign Skin Cancer and Malignant Skin Cancer. Benign skin cancer has multiple types but in this research, our focus will be on two most common types; Nevus and Seborrheic Keratosis (SK). The deadliest skin cancer is Melanoma which belongs to malignant skin cancer type. SK is a benign skin cancer derived from the non-melanocytic cells belongs to the first layer of skin [4]. Nevus also is known as dysplastic nevi (the plural of "nevus," or mole) derived from melanocytic cells of the first skin layer [5]. Melanoma is the deadliest type of skin cancer which also derives from the melanocytic cells but it can penetrate within the skin and other body parts through blood circulation [6].

Dermoscopy or microscopy is a process to capture images either through optical magnification or liquid

immersion by a dermatologist and the device is known as dermatoscopy. This device allows the better identification of different morphological features of skin lesions based on which dermatologists can decide the skin lesion type and respective treatment can be started [7]. But research also proved that accurate diagnosis of the skin lesion can be affected by the inexperience of dermatologists or by human error in this whole process [8]. Also, most of the skin lesions are quite similar in appearance e.g. there are many cases reported in the past regarding the similarity between SK and melanoma and vice versa [9]. Similarly, a typical nevus can also resemble melanoma and in some cases, people who have them are at increased risk of developing melanoma in a mole or elsewhere on the body. Although other factors are also involved in developing melanoma such as family history, poor tanning, and freckling but a still higher number of nevi will be a risk factor of turning in to melanoma [10]. To achieve early diagnoses of skin lesion, there is a need for a computerized image analysis also known as Computer-Aided Design (CAD) systems that could reduce the diagnosis error which may occur due to subjectivity and difficulty in visual interpretation [11]. Some commonly used methods are ABCD based on asymmetry, border, and color, etc. [12] and CASH algorithm [13].

Many researchers have proposed computer vision-based methods to implement such an automated system [14]–[17]. Dermoscopic images contain many types of artifacts such as hair, shadows, low contrast and background noise which will affect the process of skin lesion detection therefore these unwanted image parts will be cleaned preprocessing stage. In the second stage, the cancerous part of the image is separated from the background of the image through segmentation. Later features are extracted and selected for this segmented lesion. In the last stage, the true skin cancer type is identified by classification with the help of respective class features.

Existing methods proposed in the literature showed improvement is skin lesion detection, however, there are many challenges that must be addressed to improve the performance of such systems. A good contrast image guarantees the better accuracy of segmentation but unfortunately, most of the dermoscopic images are low in contrast with several artifacts such as hair, bubbles, and black corners, etc. The segmentation performance is also affected by several issues such as irregular and non-uniform shapes of the lesion and the occurrence of the cancerous part at the border of the image. The challenge which is faced in the feature extraction is due to highly non-uniform characteristics of the lesion such as color, size, and shape, etc. therefore the extraction of conclusive and prominent features is very important so that true skin cancer type can be classified. In the presence of these challenges, the overall performance of the system declines therefore more sophisticated techniques is required to address such issues. Also, most of the research has been done for the binary classification of skin lesion; melanoma, or benign [18][19].

In this article, we propose a statistical method for segmentation and utilize the strength of multiple classifiers. Proposed system employed the power of simple methods that are less resource-hungry yet provide better results. Following are the main contributions; proposed Delaunay triangulation with PSO for segmenting the skin lesion from pre-processed dermoscopic image, fusion of color, pattern and shape based features for the best division of skin lesion images and boost ensembling of two established classifiers for true labeling of skin lesion. Rest of the sections are organized as; section-2 describes the related work in details, section-3 elaborates the proposed methodology, section-4 presents results and discussion and paper is concluded in is presented in section-5.

2. LITERATURE SURVEY

In the preprocessing step, usually morphological operations, color space transformations, and many types of filters are used for noise removal. Dull razor software with greyscale image transformation and median filtering is used in [20] to remove artifacts such as hair, impulse, and salt and paper noise from the dermoscopic images. Color space transformation plays a very critical part in noise removal and most of the literature either uses RGB or grey-scale transformation for the implementation of noise removal techniques [18], [19], [21]. In RGB color space, every pixel of the image is represented by the value of red, green, and blue color but due to variegation of skin lesion color, this task becomes tougher. Whereas CIELAB based color space is designed to replicate a human perception of color and theoretically it carries every single color which can be perceived by human vision [22]. In [23] author processed all the images in CIELAB color space to detect suspicious melanoma colors which not only improved preprocessing but also the color channels (L, a, b) served as a color feature to improve melanoma detection. In [24] images are processed in both RGB and CIELAB color space to

improve the efficiency of melanoma detections. In [25] CIELAB based color features are used to find the probabilistic model for the automatic selection of the seed. This probabilistic model increased segmentation accuracy even in very low contrast and variable size skin lesions. Besides RGB and CIELAB, Hue Saturation and Value Management (HSV) based representation of dermoscopic images has been used as well in literature so that segmentation can be improved through better color manipulation of the lesion [26].

Many statistical-based techniques have been implemented in the past for the segmentation task. Delaunay triangulation based methodology is used with edge detection in [27] to improve segmentation accuracy. They used the Canny algorithm to calculate the edges given as input to Delaunay procedure which tessellate the triangles of an image then HSV based color averaging is calculated for each triangle to separate the lesion. Delaunay triangulation is also used in [28] where this technique is utilized to extract the binary mask of the cancerous part of the image and it doesn't require any type of training. But in recent times not much work is done in this application which involves Delaunay and HSV based techniques. In [29] six techniques based on clustering, edge-based, and thresholding are used for the segmentation of 100 dermoscopic images. Saliency mapping is another statistical technique that is used in [30] where the lesion is segmented by color, region, and boundary-based characteristics of the foreground. The same techniques are also used in [31] where Otsu thresholding is incorporated with other characteristics for more effective map calculations. GrabCut algorithm is used for the skin lesion segmentation in [32] where boundary conditions are improved with the color features training and K-means clustering. In [33] segmentation is performed through the clustering-based method and level set algorithm. In the beginning, the clustering-based method is used to initialize segmentation then level set theory incorporated to refine the results. In [34] a hybrid approach is used to segment the lesion from images. They used Otsu based thresholding in the beginning then the active contour-based technique is incorporated with level set theory to segment the foreground from images. In [35] a review of the latest segmentation techniques is presented and a new segmentation method is also proposed that used clustering and local binary methods to identify the boundaries of lesion.

Extracted features from dermoscopic images play a key role in classifying true lesion type. Usual features of skin lesions include color, size, shape, histogram, contour, and border, etc. In [36] a survey is done on features of skin lesion which are divided into three main categories; hand-crafted features which include color, texture, and shape-based feature. The second category is local and global features, the third category is clinical features which are calculated based on ABCD rule, 7-point checklist, and Menzies rule, etc. In [37] texture, color, and Histogram of Oriented Gradients (HOG) based features were fused and selected through the Boltzman Entropy-based algorithm, selected features were given input to SVM based classifier. Clinical features and patient metadata is used in [38] to develop a multimodal classifier based on convolution neural networks for binary classification. In this research, it is also proved that the proposed classifier performed better with dermoscopic images as compared to microscopic images. In [39] author used Gabor filter, Grey Level Co-occurrence Matrices (GLCM), HOG, and Local Binary Patterns (LBP) to extract texture-based features. Then Multilayer Perceptron (MLP) based classifier implemented to classify between melanoma and non-melanoma skin lesion. In [18] author optimized conventional features such as HOG, GLCM, color, and LBP. After fusion and selection from these optimized features, classification is performed through different kernel functions of SVM. In [19] a hybrid of statistical and machine learning is proposed to extract the features. Optimized color features are extracted through VGG and AlexNet models later classification is done through neural networks. In [40] shape, color, and texture-based features are extracted through LBP and Kirsch operator. Classification is implemented through modified PSO where the search mechanism is modified by the firefly algorithm which is a probabilistic distribution-based model.

3. PROPOSED METHODOLOGY

In this section, complete methodology is discussed. Figure. 1 shows the flow diagram of proposed method to detect true skin lesion type. Further steps that are part of proposed methodology are discussed in following sub sections.

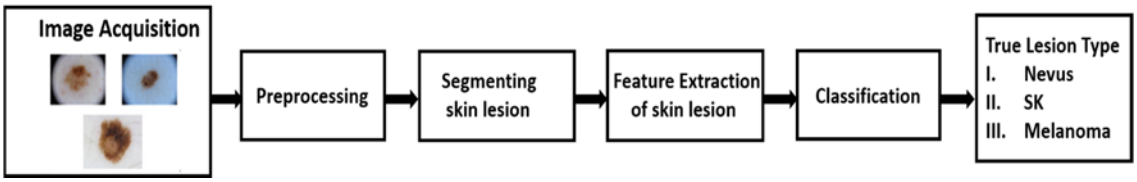

Figure. 1: Flow Diagram Of Proposed Methodology

3.1 Preprocessing

Preprocessing is considered as the first and most important step in the process of detecting the true skin lesion type from the dermoscopic images. This step is important for making the desired area more prominent and reducing unwanted noise like artifacts and small dots etc. We have combined multiple techniques for preprocessing the original noisy image. Initially, we applied local contrast enhancement on the image to improve the contrast which makes the diseased region more prominent. Following this, a statistical method of haze reduction is applied on CIELAB color space of the image that uses mean and standard deviation to enhance the overall image. Overall contrast enhancement is carried out through following equation 1.

$$E(x,y) = \mu(x,y) + \varphi(x,y)O(x,y) - \mu(x,y)) \quad (1)$$

Where E is local contrast enhanced image, μ represents mean and φ is the contrast gain used in ACE algorithm as explained in [41]. Incorporating this enhancement method improves the overall contrast of the skin lesion image by making the cancerous part more prominent.

In order to increase the visibility of foreground the RGB image is converted in to CIELAB color space in the second stage of preprocessing CIELAB color space is preferred over RGB because it carries every single color which can be perceived by human vision [22]. It defines the brightness in the form of L from black to white and the value of a and b defines the ranges from green to red and blue to yellow, respectively. Direct conversion from RGB to CIELAB is not possible and first, it needs to be transformed from RGB to XYZ tristimulus with the selection of a white point in the image and gamma function. Gamma function is method utilized to linearize simple RGB image components when transforming them into a linear space, further explanation can be found in [42].

In final stage of preprocessing, haze reduction is applied on CIELAB image to improve the quality of the foreground and make it more separable from the background. For the improved version of the output image, the brighter channel can be improved by darker channel first dehazing operation as shown in equation. 2.

$$OH(x) = H_f(x)e - \nabla d_s(x) + A(1 - e - \nabla d(x)) \quad (2)$$

Where delta x shows the local patch of the image, OH is the observed hazy image, H_f is the haze-free image, A is the atmospheric light, d_s is scene depth, and ∇ is the scattering coefficient of the environment. Further explanation can be found in [43]. The progression of skin esion enhancement through preprocessing on sample images from ISIC dataset is shown in Figure. 2.

3.2 Image Segmentation

The purpose of image segmentation is to split the original image into multiple segments that are called as foreground and background in this case. The foreground is separated from the background based on color and shape features similarity. We proposed a method that combines Delaunay clustering with PSO. Further, HSV value based thresholding is incorporated in second stage of segmentation.

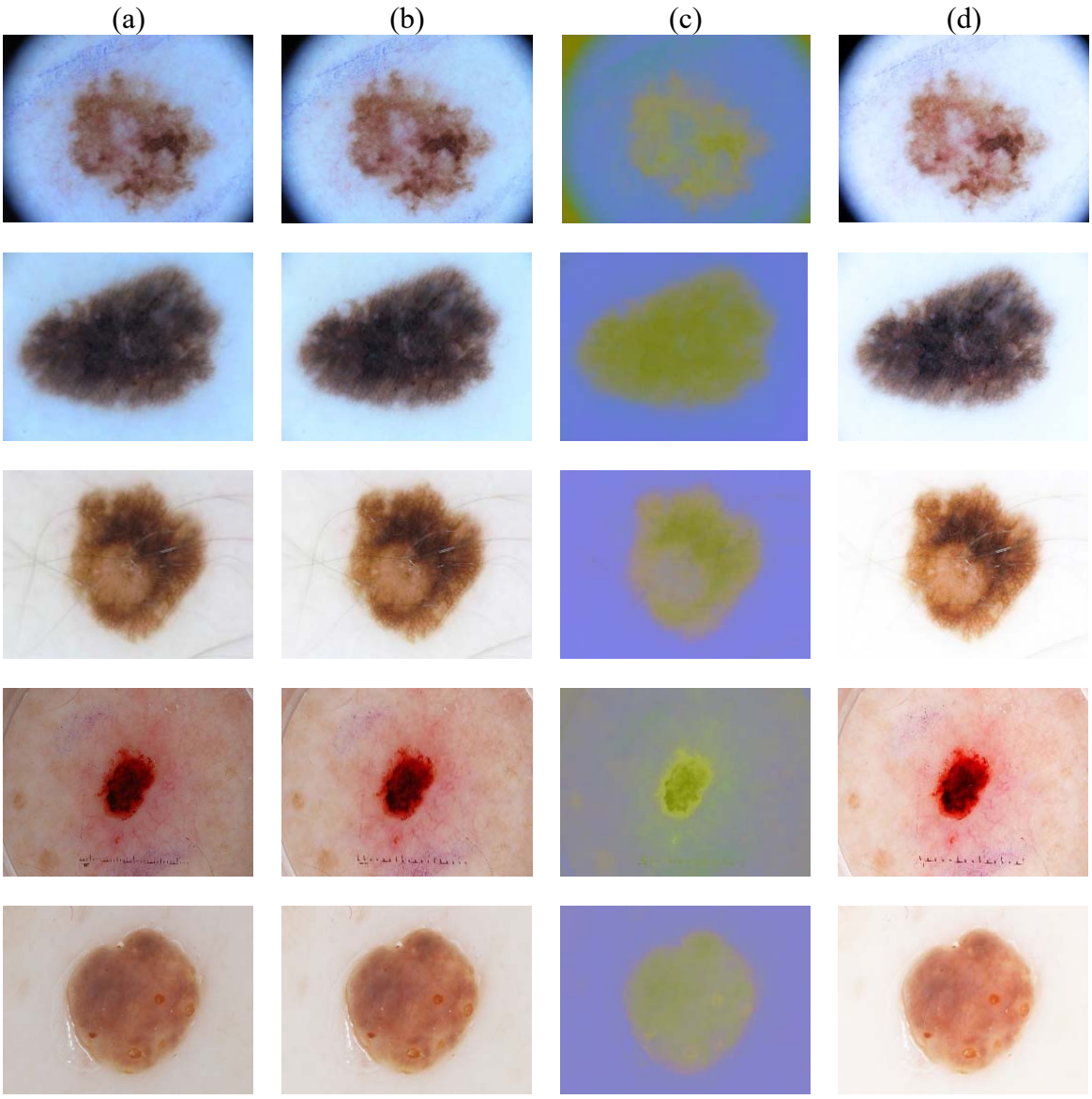

Figure. 2: Skin Lesion Enhancement Through Preprocessing: (a) Original Image, (b) Local Contrast Enhanced Image, (c) CIELAB Converted Image, (d) Haze Removed Image

3.2.1 Delaunay triangulation based clustering

Most of the existing clustering methods used in segmentation have some known limitations mainly due to variable size, density value, noise and shape of the lesions. These approaches are flaw-able for non-linear data. We employed an extended version of Delaunay that will perform the clustering in spatial domain called Delaunay triangulation for spatial clustering. Experimental results show that this technique achieves promising results for clustering and separability problems in applications of computer vision [44].

Delaunay triangulation converts high dimensional data of polygons and polyhedral into triangles. It divides the overall space by joining the dots on the 2D plane by drawing triangles in a way that the smallest point of the inner angles of connecting triangles is maximized, and every split triangle is almost an equilateral. Consider the set of

multiple points S={p_1,….p_N}with each point having x_iand y_i. Triangulation of these points can be defined as, DT(q)={d_1,….d_H }. Each T represents the set of points of each triangle. H represents total triangles that are maximum 2N-2 as per point data distribution.

After grouping the diseased pixel using Delaunay triangulation, we exploited a novel and recognized method for optimization of the segmented region called PSO. It is a mathematical algorithm that makes assumptions about the algorithm being optimized in our case clusters of Delaunay triangulation. Further, it does not require any gradient calculation and works based on population (swarm) and candidate (particle). According to the formulation of PSO, the particles are displaced in the allowed range based on their best-known position and best swarm position. The process of movement is repeated until the best clusters are formed for segmentation.

3.2.2 Hues, Saturation and Value arrangement (HSV)

Conversion of RGB image to HSV domain results into three elements, H (hue) is the actual color pigment in 360 rotations, S (saturation) shows the concentration of color from 0 to 100 and V (value) tells how bright the color is from range 0 to 100. From the output images in Fig. 2(d) it can be easily considered that all the diseased regions have specific brunt dark reddish and brownish representation and using some specific threshold (39, 88, 90) after multiple experiments, we extracted the melanoma region and applied binary thresholding which is translated over original dermoscopic image to outline the segmented lesion. The step by step visual output of sample images during segmentation process is shown in Figure. 3.

3.3 Feature Extraction

Following features are extracted from the segmented images to perform the classification task.

3.3.1 Color Histograms

Color histogram creates different bins based on the color frequency distribution within the image. The pixels having similar values are being collected and then stored. This process has been done with the help of two different types of histograms; the first one is the global histogram and the second one is the local histogram. A global histogram is used to define the global descriptors of the particular image to solve the problems of image rotation, change in translation, or angle view. In the local histogram, the main focus is on the spatial features of the image at the pixel level. Histogram intersection is employed to separate the features of local as well as global histograms. It is defined in equation 3.

$$HI(x,y) = \sum_{i=1}^{n} \text{MinOrMax } [(x_i, y_i)] \quad (3)$$

Here x and y represents the value of the pixels, whereas i is the counter which goes from the first pixel to the total number of pixels. MinOrMax function is used collectively for the local and global histogram. By using equation 3, color histograms values which belong to global descriptors are sorted using the max function of the equation 3. Whereas, local histogram values are sorted using the min function of the equation 3. These features are particularly useful in segmentation because the particular patch of the cancerous part in the image has the absolute color scheme. The reason behind the selection of the features of HSV is that these are resilient against the noise of the image. We selected 90 features by creating the 4 bins of H (360 values) and 25 features for each V and S. This created 140 overall features that are then passed to the fusion layer for classification purposes.

3.3.2 Local Binary Patterns (LBP)

Local Binary Pattern (LBP) is used to extract the texture information from the image. For skin lesion problem, LBP is used to identify the segmented area based on the texture of the cancerous region. The local binary patterns are based on the four different parameters which are as follows:

1. *Circular radius*: The value of the central pixel in the radius is set to 1 to define the circular area of the local binary pattern.
2. *Neighborhood pixels*: The neighbor pixels are used to set the circular boundary around the central pixel. The selected number of neighborhood pixel are 8. If the number of neighbor pixels are increased, the computational power also increases.
3. *X grid*: X grid represents the number of pixels in the cells which are placed in the horizontal direction. The finer Local Binary pattern features depend upon the vast dimensionality, and number of cells. The more the cells, more the finer features. Hence 8 is selected as this parameters.

Journal of Theoretical and Applied Information Technology
15th March 2021. Vol.99. No 5

ISSN: 1992-8645 www.jatit.org E-ISSN: 1817-3195

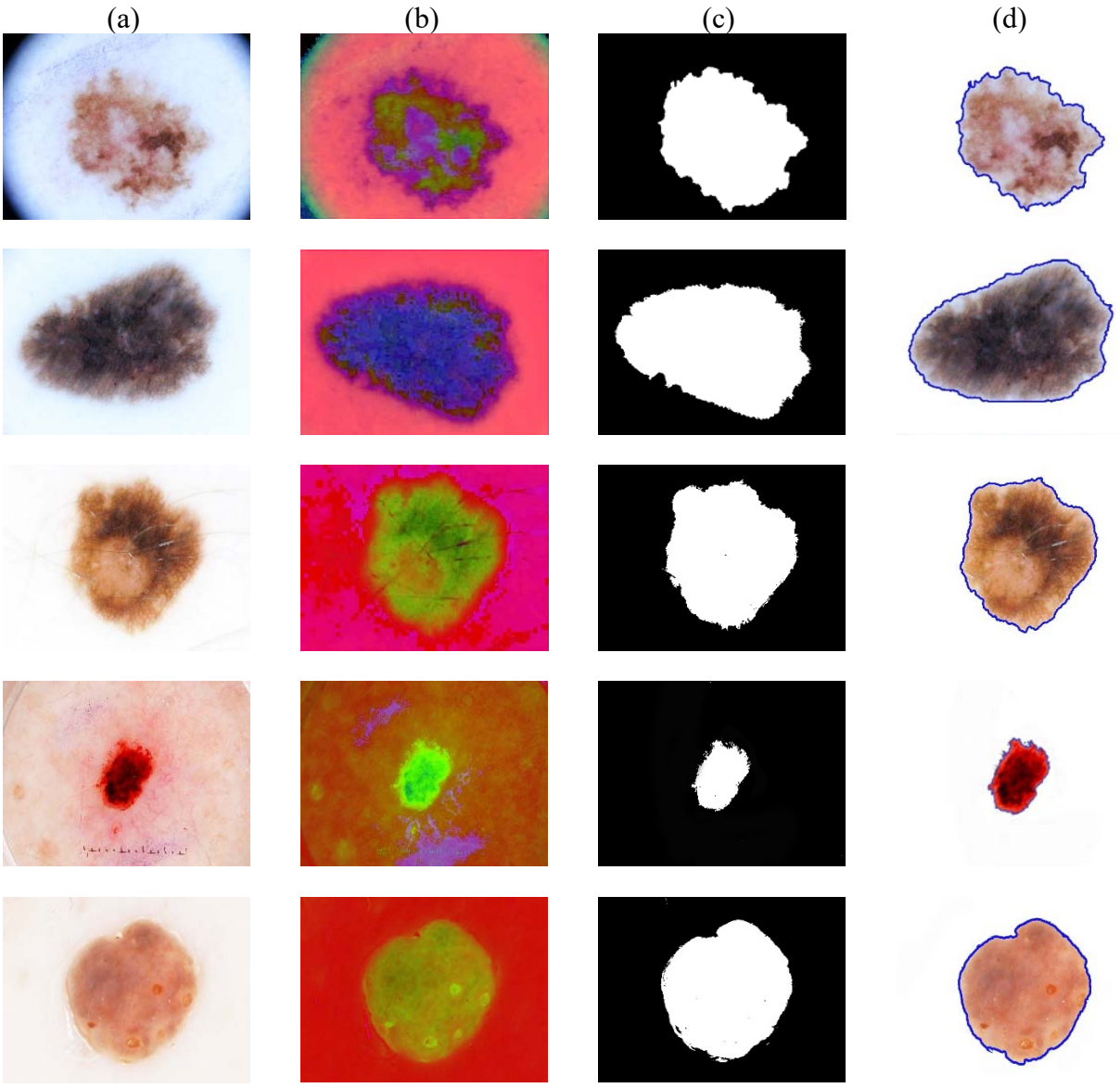

Figure. 3: Segmentation Results by Proposed Method: (a) Input Image For The Segmentation Process (b). Image After HSV Thresholding, (c) Binary Image, (d) Segmented Image

Y grid: The Y grid represents the pixel present in the cells placed in the vertical direction. dimensionality, we select. Through experiments it is also set to 8 for good feature selection.

In this phase, the algorithm labeled the pixels of the particular frame to identify the segmented region of the skin lesion. The kernel with the size of 3×3 has been convolved on it, to find the central pixel point of this filter. The pixel values are converted into binary values. These binary values are then separated based on some specific threshold into high and low values. In the end, these values are converted into the decimal value for better feature extraction of the segmentation process. Each input segmented image has been divided into four 4x4 blocks, and local edge histograms are computed for each of the blocks as shown in Figure. 4. From each block, the algorithm selects the 16 dimensional vectors. Finally, 64 dimensional vectors or features are produced to represent the edges information in the frame.

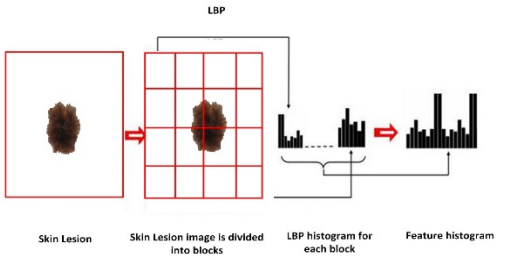

Figure. 1 Feature Extraction Through Local Binary Patterns

3.3.3 The Hough transform

To identify the region of the shape, the Hough transform has been utilized. To implement the Hough transform, edge points are identified. A canny edge detector has been utilized for the edge points. It is based on the four different steps which are as follows:

- Reduction of the Noise
- Calculation of the gradient
- Non-maximum suppression
- Doubling the threshold

Gaussian blurring techniques have been utilized to remove the noise from the frame. Gradient descent technique identifies the edges from the blurred image, which we get from the convolution process. The principle behind this algorithm is that algorithm scans all values of the matrix having the gradient intensity. After that, it searches the values having the maximum edge intensity in the defined direction. The algorithm checks the direction of the edge pixels and processes only those pixels which are in the same direction as the edge pixel.

The Hough transform uses these edge features, and draws a line then finds out the intersection. The intersection points give us the shape features of segmented lesion. We set the threshold value for the selection of the shape features based on the intersection value. Selection is made on 10 points (x, y) using this criterion, making 10 features that are passed to fusion layer.

3.4 Early Fusion

All the features from the above feature extraction methods are combined to create a hybrid vector that represents the overall heterogenic feature space by including color, texture and shape properties. From color histogram 140 features are secured which are combined with the other 64 features of LBP histograms, making the overall features count to 204. We also captured a specific list of 10 features from the Hough method that makes our overall length of the feature vector as 214 features. All these features collectively represent the heterogenic properties of the skin lesion.

3.5 Classification

Features of 214 sizes are used by the classification module which finally identifies the true type of skin lesion based on the extracted region in segmentation. We exploited the power of early fusion and late fusion with bagging for improving the overall accuracy.

3.5.1 Support Vector Machine

SVM draws a hyperplane to separate the data points. There can be multiple hyperplanes that potentially separate the points but an optimal plane is that maximize the margin in a way that the distance between support vectors of opposite classes should be maximum. Support vectors are the nearest observation of the hyperplane that can be defined as given in equation 4.

$$w_v \cdot x + b = 0 \quad (4)$$

Where w_v the normal on the plane and b is the offset of the plane from origin and x is the input features vector. SVM with the guassian radial base kernel is employed for training on half of the dataset, 1000 images. The following equation 5 shows the radial basis kernel.

$$K(a_1, a_2) = \exp(\gamma (a_1 - a_2)^2) \quad (5)$$

Where K is the kernel and a_1 and a_2 are feature vectors and γ is gamma the hyper parameter that is used for smoothing of the decision boundary. We have employed SVM as our first classifier for late fusion using the ensemble learning method. SVM is initially trained on half of the dataset based with 214 features of early fused. All the instances are passed from the SVM model with the gamma parameter set to 0.1 after different attempts. After generalization, the model predicted correct labels on most of these images, and the remaining images are separated to be trained on the second classifier type. Further explanation is given in the section explaining ensemble learning.

3.5.2 Aritificial Neural Network (ANN)

Suppose, x vector represents the input to the neuron. Each explicit input is further multiplied with the weight matrix represented by

Journal of Theoretical and Applied Information Technology
15th March 2021. Vol.99. No 5

ISSN: 1992-8645 www.jatit.org E-ISSN: 1817-3195

$w_1, w_2, w_3, \ldots, w_n$. After multiplication with the weight matrix, the resultant product is summed over all the products with the sum of bias factor b. An activation function is applied to the resultant signal. The basic motive behind using the activation function is to introduce non-linearity in the signal.

We employed a Rectified Linear Unit (RELU) [45] as the activation function in our network for the classification of the skin lesion in image. The RELU activation function is defined by equation 6.

$$f(x) = \begin{cases} 0, & x < 0 \\ x, & x \geq 0 \end{cases} \quad (6)$$

Multiple neurons are combined in a hidden layer. These layers learn based on gradient descent during backpropagation. There are different optimizers for updating the weight matrix; we utilized Adam optimizer function for optimizing the weights of hidden layers. We employed a four-layered Multi-Layer Perceptron (MLP) method as a classifier after SVM. A set 214 features are transformed using a set of linear layers to 128 features using the first layer of 512, followed by 256 and 128 neurons units in the second and third layers, respectively.

3.5.3 Boosting Ensemble Learning

This process is used to generate multiple predictions and later on combine these predictions. Two models learn as weak classifier with their optimization process. At the same time, the third classifier is built at every step to improve the overall accuracy. The basic flow of the boosting process is as follows,

- Extract a random sample set s_1 with no replacement from a bigger training set and train the first weak learner that is SVM.
- Again extract a second randomized sample set s_2 from the original set. Using this small set to train the second weak learner (SVM).
- Finally, extract another subset to train the third weak learner (MLP).
- In the end, combine all the trained weak learners based on weighted majority voting.

We have used SVM as the first and second learner and ANN (MLP) as the third leaner. Initially, both SVM classifiers train on subset followed by an ANN network trained on the data where both SVMs contradicts because of data randomness. The voting mechanism is shown in equation 7.

$$H(x) = \sum t = 1 * T\, w_t\, l_{t(x)} \quad (7)$$

Overall hypothesis H is the weighted sum of all the weak learners. Where l_t and w_t are a weak learner and weight matrix respectively. For loss function, we have employed cross-categorical cross-entropy as the loss function. In Figure. 5 the true label and output predicted results of classifier on ISIC dataset is presented. Proposed architect of end to end system from preprocessing till classification is presented in Figure. 6.

4. RESULTS AND DISCUSSION

The proposed system generates output in three forms. One is the binary image that depicts the foreground and background region of skin lesion segmentation. Second is the segmented region from the original RGB skin lesion image and the third output is the class label for that segmented region. There are two publically available datasets that have been employed to train and evaluate the performance of proposed model. International Skin Imaging Collaboration (ISIC) is one of those biggest databases accessible publically comprising of 2000 visual instances with classification and segmentation details of skin lesion [46]. From the 2000 visual data, 254 images are SK, 1372 as nevus, and remaining 374 images are analyzed as melanoma. This dataset comprises images of skin lesions from all the speculated body parts, which were gathered from various sources, because of this explanation the size, aspect ratio, and illumination of all the medical images are unique. PH2 [47] is second database which has been used for the evaluation of segmentation. It comprises of 200 dermoscopic images alongside the comparing clinical explanations, containing 40 malignant melanomas, 80 atypical nevi and 80 normal nevi.

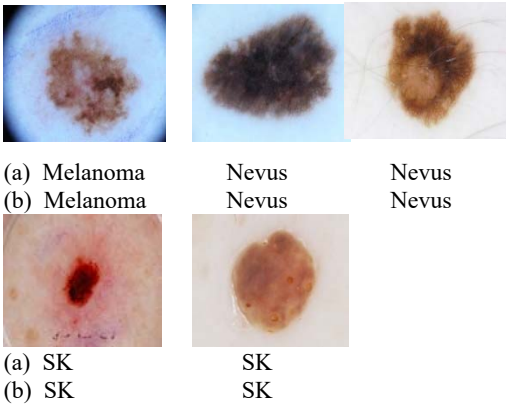

Figure. 5: Classification Results on ISIC dataset: (a) True Label, (b) Predicted Label

Journal of Theoretical and Applied Information Technology
15th March 2021. Vol.99. No 5

ISSN: 1992-8645 www.jatit.org E-ISSN: 1817-3195

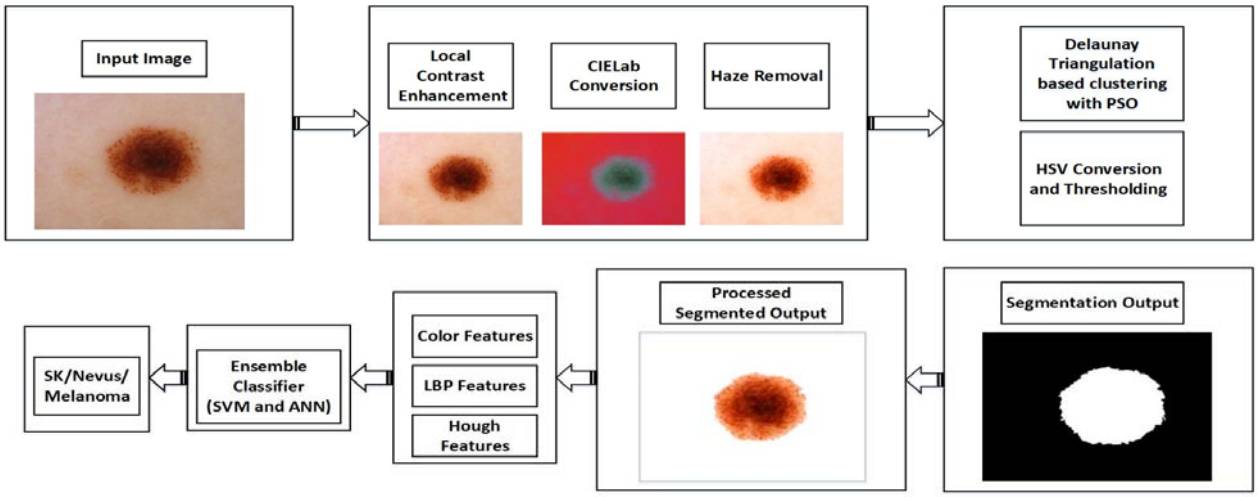

Figure. 6: Proposed Architect Of The System For Skin Lesion Segmentation And Classification

Segmentation lesion results are evaluated by comparing the outcome with the ground truth segmented images of two benchmark datasets PH2 and ISIC. The segmented ground truth label images in these datasets have been generated by professional dermatologists. Similarly, skin lesion type classification is compared with class labels provided with ISIC dataset. Segmentation performance and fidelity are measured using accuracy, True Negative Rate (TNR) and True Positive Rate (TPR). However, classification is evaluated using multiple metrics including accuracy, False Negative Rate (FNR), Precision, Recall, F1-score, and Response time. Segmentation and classification evaluation are discussed in the following sections.

4.1 Segmentation Evaluation

These performance metrics can be denoted in the form of equations. Segmentation accuracy can be stated as pixel accuracy and can be illustrated as shown in equation 8.

$$\mathrm{Acc}_{\mathrm{seg}} = \frac{n_{TP} + n_{TN}}{n_{TP}+n_{TN}+n_{FP}+n_{FN}} \quad (8)$$

Where n_{TP} and n_{TN} represent number of pixels accurately classified as foreground and background respectively. Moreover, n_{FP} and n_{FN} represent the number of pixels incorrectly considered as foreground and background, respectively. The TPR or sensitivity of the segmentation algorithm can be defined as shown in equation 9.

$$\mathrm{TPR} = \frac{n_{TP}}{n_{TP}+n_{FN}} \quad (9)$$

Also, the TNR or specificity of the segmentation is calculated to evaluate the ratio of actual foreground pixels that are accurately detected and can be calculated as shown in equation 10.

$$\mathrm{TPR} = \frac{n_{TN}}{n_{TN}+ n_{FP}} \quad (10)$$

Table 1 shows the confusion matrix of the ISIC dataset and Table 2 shows the confusion matrix for PH2 dataset. A confusion matrix is formulated by averaging the ratio of each n_{TP}, n_{FN} and n_{FP}, n_{TN} with the number of actual positive and negative number pixels, respectively. Table 1 shows that the proposed segmentation technique accurately classifies foreground pixels with true positive accuracy of 97.6% and background pixels with true negative accuracy of 95.9%. The table indicates the more background pixels are considered as foreground pixels than foreground pixels regarded as background. Such results are demanding because no information regarding melanoma regions will be dropped. Similarly, Table 2 shows the segmentation results on the PH2 dataset which depicts that 95.3% of foreground pixels are filtered out correctly while 4.7% of pixels from the foreground are misclassified as background, hence some loss of information. Likewise, results on ISIC, more of background pixels are regarded as foreground pixels.

Table 1: Confusion Matrix For Segmentation On ISIC Dataset

ISIC	Foreground	Background
Foreground	97.6%	2.4%
Background	4.1%	95.9%

Table 2: Confusion Matrix For Segmentation On PH2 Dataset.

ISIC	Foreground	Background
Foreground	95.3%	4.7%
Background	11.2%	89.8%

A comparison of the proposed segmentation technique with some renowned benchmarks from literature with respect to accuracy, TNR and TPR is presented in Table 3. Proposed algorithm has been tested for both datasets as shown in Table 3. From Table 3 we can interpret that the proposed method has achieved segmentation accuracy of 96.8% and 92.1% for ISIC and PH2 database respectively, better than statistical methods and deep learning-based models. In terms of sensitivity (TPR) and specificity (TNR), proposed techniques secured better results than

Table 3: Comparison Of Proposed Segmentation Technique With Benchmark Techniques

Paper	Accuracy (%)	TNR (%)	TPR (%)	Dataset
[32]	91.9	98.5	80.5	ISIC
[31]	93.6	-	87.0	PH2
[28]	89.6	97.2	80.2	PH2
[18]	96.0	-	-	ISIC
[48]	94.6	-	-	ISIC
[19]	94.4	90.0	92.0	ISIC
[49]	93.8	96.4	87.0	ISIC
Proposed	96.8	97.6	95.9	ISIC
Proposed	92.1	95.0	89.5	PH2

Delaunay triangulation [28], other statistical based benchmark methods and deep learning [19] based method for segmentation.

The sensitivity value indicates the ability of segmentation technique to accurately distinguish cancerous region pixels from other skin region pixels. Whereas, the specificity tells about the ability to accurately discard the skin region pixels to be considered as a cancerous region. That can later cause misclassification in skin melanoma type recognition. Hence, accurate segmentation is necessary for correct classification. Other than comparable accuracy with state of the art techniques, proposed techniques do not require any computational complexity as in deep learning-based algorithms. As we can interpret from Table 3 that performance on PH2 database is compelling on that is trained using ISIC dataset. If we employ the PH2 dataset to train the same methodology, we can achieve better performance on PH2 database as well. Visual segmentation results on ISIC and PH2 datasets are presented in Figure. 7 and Figure. 8 respectively. In these figures input images are presented in first column, the second and third columns show the predicted output by proposed technique and ground truth image respectively. The final column shows the difference in the ground truth and predicted output by drawing red lines on predicted output and green lines on the ground truth image. When analyzed closely it is observed that the false positives are higher than the false negatives. Hence, the impact on false classification will be reduced.

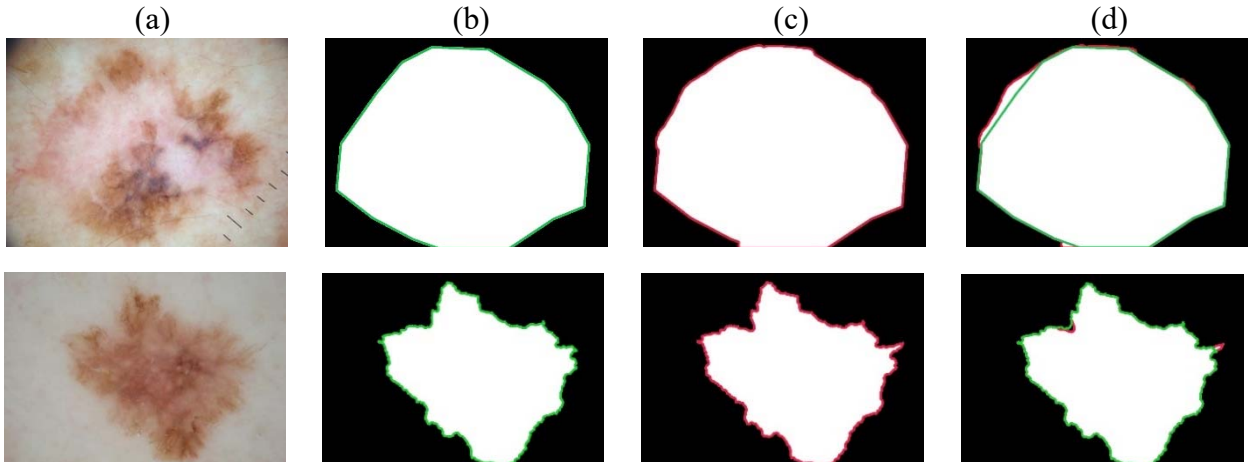

Figure. 2: Segmentation Results For ISIC Dataset: (a) Original Image, (b) Ground Truth Output, (c) Predicted Output, (d) Difference In The Ground Truth And Predicted Output

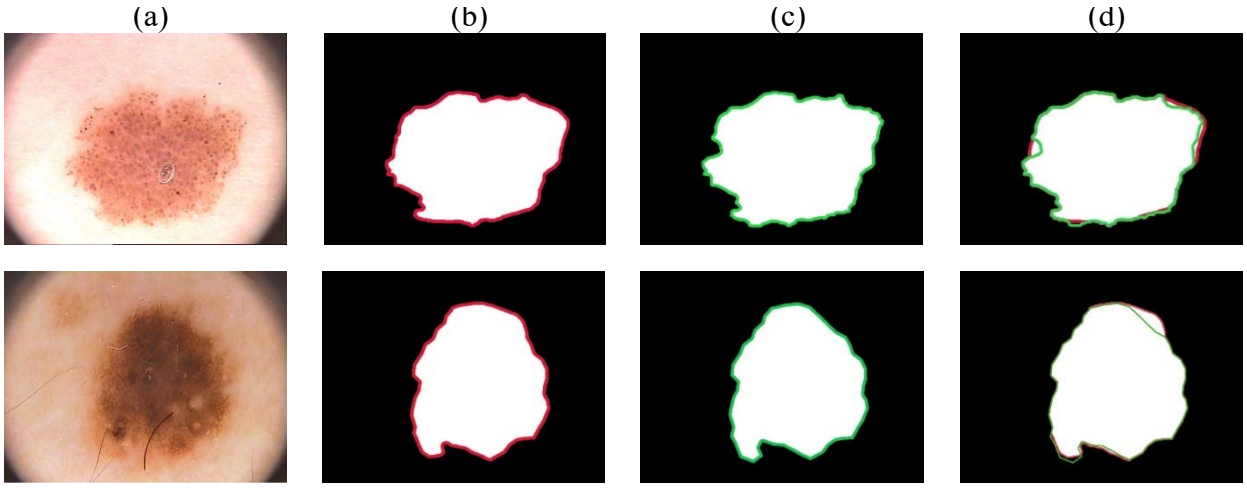

Figure. 8: Segmentation Results For PH2 Dataset: (a) Original Image, (b) Ground Truth Output, (c) Predicted Output, (d) Difference In The Ground Truth And Predicted Output

4.2 Classification Evaluation

The proposed methodology computes color, LBP and Hough features from segmented images. The fusion of these features is performed to train the ensemble classifier. The classification results of the proposed classification technique are measured in following three ways.

- Single SVM Classifier
- Single MLP Classifier
- Ensemble SVM and MLP

For all these three ways, a set of features remains the same. To train these classifiers, 10-fold cross-validation is employed. Dataset is divided into ten sets and one set is kept for testing and the classifier is trained for the rest of nine sets. The process is adapted 10 times and results are computed as an average of all 10 rounds. A confusion matrix for the classification performance is shown in Table 4.

Table 4: Confusion Matrix For Classification On ISIC Dataset.

ISIC	Melanoma	Nevus	SK
Melanoma	97.6%	0.8%	1.6%
Nevus	1.5%	97.3%	1.2%
SK	0.7%	0.5%	98.8%

Table 5 presents the results of the ISIC dataset when experiments are made on three classification algorithms with the same features set. Table 5 measures the performance of each classifier using the evaluation metrics shown in equation 11 to 14.

$$\text{Precison} = \frac{n_{TP}}{n_{TP} + n_{FP}} \quad (11)$$

$$\text{Recall} = \frac{n_{TP}}{n_{TP} + n_{FN}} \quad (12)$$

$$F_1 = \frac{2*(\text{Recall}*\text{Precision})}{\text{Recall}+\text{Precision}} \quad (13)$$

$$\text{FNR} = \frac{n_{FN}}{n_{TP} + n_{FN}} \quad (14)$$

Where n_{TP}, n_{FP} and n_{FN} denote the number of true positive, false positive, and false negatives according to classification output, respectively. Results in the Table 5 show the superiority of the proposed ensemble classifier over single classifiers. The proposed classifiers achieve the highest accuracy of 97.9% on the ISIC dataset.

Table 5: Classification Results Of Proposed Techniques

Classifier	Accuracy (%)	FNR (%)	Precision	Recall	F1-Score
SVM	92.2	7.8	92.0	92.4	92.1
MLP	93.5	6.5	93.2	93.8	93.4
Ensemble SVM & MLP	97.9	2.1	97.2	98.0	97.0

Moreover, to prove the performance of the proposed classification technique along with robust features, a comparison is made with previous techniques from the literature, presented in Table 6. The classification results of the proposed methodology, through ensemble of SVM and MLP, are better than the chosen recognized benchmark techniques as shown in Table 6. The comparison has been made with two deep learning-based techniques [19], [38] and one statistical technique [18] on ISIC dataset. The proposed method achieves 97.9% of classification accuracy which is a lot more than deep learning based technique presented in [38]. Additionally, the response time of the proposed method is slightly higher than [19] but is less than the statistical approach presented in [18]. Proposed classifier also exhibit much better performance with respect to TNR and TPR as compare to both deep learning and statistical based methods.

All the visual and numerical analysis presented in this research verifies the better performance of proposed system but more improvements can be brought up especially with respect to computational cost. In future a system can be proposed without pre-processing step as many articles in literature [38] are doing the same to reduce computational cost but this change might will reduce the accuracy. Hence a tradeoff needs to be developed between computational cost and segmentation, classification accuracies.

Table 6: Comparison Of Proposed Classification Technique With Benchmark Techniques

Paper	Accuracy (%)	TNR (%)	TPR (%)	Response Time(s)	Dataset
[19]	96.5	97.0	96.5	16.46	ISIC
[18]	93.7	95.0	93.3	38.61	ISIC
[38]	72.1	-	-	-	ISIC
Proposed	**97.9**	**98.0**	**97.2**	**20.44**	**ISIC**

5. CONCLUSION

In this paper, we present a new statistical method for skin lesion segmentation and classification. The proposed technique is employed in three steps i) Preprocessing ii) Image Segmentation iii) Feature extraction and Image Classification. Preprocessing is carried out by removing noise and artifacts from the dermoscopic images using
CIELAB conversion. Later, this paper proposes a novel technique using Delaunay triangulation spatial based clustering with PSO followed by HSV color space adjustments to segment skin lesion region from the background region. We propose a set of robust color, texture and shape based features to be extracted from the segmented image. Histogram, LBP and Hough features are extracted to form a set of 214 features. These features are passed to two weak SVM classifiers and then ensemble to train another ANN classifier. Finally, the outcome of the classifier is measured in the form of a probability score per class. Our proposed method achieves the

accuracy compared to the state of the art statistical as well as deep learning based techniques with a segmentation accuracy of 96.8% and 92.1% for ISIC and PH2 datasets respectively. Classification accuracy of 97.9% on ISIC dataset is accomplished as well. More segmentation results have also been presented for the PH2 database as well. Besides accuracies proposed method has lower response time as compare traditional statistical methods in literature which prove the efficiency of traditional low-level techniques but still it is higher than deep learning based methods. Overall it can be concluded that proposed technique performed better than latest statistical and deep learning based methods with respect to segmentation and classification accuracies.

REFERENCES:

[1] R. L. Siegel, K. D. Miller, and A. Jemal, "Cancer statistics, 2019," CA. Cancer J. Clin., vol. 69, no. 1, pp. 7–34, Jan. 2019, doi: 10.3322/caac.21551.

[2] B. E. Vasicek, S. M. Szpunar, and L. A. Manz-Dulac, "Patient knowledge of sunscreen guidelines and frequency of physician counseling: A cross-sectional study," J. Clin. Aesthet. Dermatol., vol. 11, no. 1, pp. 35–40, Jan. 2018.

[3] D. Mocellin, S. and Nitti, "Cutaneous melanoma in situ: translational evidence from a large population-based study," AlphaMed Press, vol. 16, no. 6, p. 896, 2011, Accessed: Jan. 22, 2019. [Online]. Available: http://theoncologist.alphamedpress.org/content/early/2011/05/14/theoncologist.2010-0340.short.

[4] U. Wollina, "Seborrheic Keratoses – The most common benign skin tumor of humans. Clinical presentation and an update on pathogenesis and treatment options," Open Access Maced. J. Med. Sci., vol. 6, no. 11, pp. 2270–2275, Nov. 2018, doi: 10.3889/oamjms.2018.460.

[5] X. Wang, Q. Liu, L. Wu, Z. Nie, and Z. Mei, "Risk of non-melanoma skin cancer in patients with psoriasis: An updated evidence from systematic review with meta-analysis," J. Cancer, vol. 11, no. 5, pp. 1047–1055, 2020, doi: 10.7150/jca.37015.

[6] A. C. Halpern, A. A. Marghoob, A. J. Sober, V. Mar, and M. A. Marchetti, "Clinical Presentations of Melanoma," in Cutaneous Melanoma, Springer International Publishing, 2020, pp. 107–144.

[7] M. Janda et al., "Accuracy of mobile digital teledermoscopy for skin self-examinations in adults at high risk of skin cancer: an open-label, randomised controlled trial," Lancet Digit. Heal., vol. 2, no. 3, pp. 129–137, Mar. 2020, doi: 10.1016/S2589-7500(20)30001-7.

[8] C. P. H. Reinehr and R. M. Bakos, "Actinic keratoses: review of clinical, dermoscopic, and therapeutic aspects," An. Bras. Dermatol., vol. 94, no. 6, pp. 637–657, Nov. 2019, doi: 10.1016/j.abd.2019.10.004.

[9] C. Oliveira, A., Arzberger, E., Massone, C., Carrera, "Verrucous melanoma simulating melanoacanthoma: dermoscopic, reflectance confocal microscopic and high-definition optical coherence tomography," Australas. J. Dermatol., vol. 57, no. 1, pp. 72–73, 2016, Accessed: Jan. 22, 2019. [Online]. Available: http://repositorio.chlc.min-saude.pt/bitstream/10400.17/2708/1/Australas J Dermat 2016.pdf.

[10] C. F. Gandini, S., Sera, F., Cattaruzza, M.S., Pasquini, P., Abeni, D., Boyle, P. and Melchi, "Meta-analysis of risk factors for cutaneous melanoma: I. Common and atypical naevi," Eur. J. Cancer, vol. 41, no. 1, pp. 28–44, 2005, Accessed: Jan. 22, 2019. [Online]. Available: https://www.sciencedirect.com/science/article/pii/S0959804904008329.

[11] D. Moreno-Ramírez et al., "Increasing Frequency of Seborrheic Keratosis Diagnoses as a Favorable Consequence of Teledermatology-Based Skin Cancer Screening: A Cross-sectional Study of 34,553 Patients," Am. J. Clin. Dermatol., vol. 18, no. 5, pp. 681–685, Oct. 2017, doi: 10.1007/s40257-017-0283-z.

[12] N. G. Marghoob, K. Liopyris, and N. Jaimes, "Dermoscopy: A review of the structures that facilitate melanoma detection," Journal of the American Osteopathic Association, vol. 119, no. 6. American Osteopathic Association, pp. 380–390, Jun. 01, 2019, doi: 10.7556/jaoa.2019.067.

[13] I. Zaqout, "Diagnosis of Skin Lesions Based on Dermoscopic Images Using Image Processing Techniques," in Pattern Recognition - Selected Methods and Applications, IntechOpen, 2019.

[14] M. Celebi, H. Iyatomi, and W. Stoecker, "Automatic detection of blue-white veil and related structures in dermoscopy images," Comput. Med. Imaging Graph., vol. 32, no. 8, pp. 670–677, 2008, Accessed: Jan. 22, 2019. [Online]. Available:

https://www.sciencedirect.com/science/article/pii/S0895611108000815.

[15] T. Saba, S. Al-Zaharani, and A. Rehman, "Expert System for Offline Clinical Guidelines and Treatment," Life Sci. J., vol. 9, no. 4, pp. 1097–8135, 2012, Accessed: May 27, 2020. [Online]. Available: http://www.lifesciencesite.comhttp//www.lifesciencesite.com393.

[16] I. A. J. A. Y. M. M. M. Nida N, "Melanoma lesion detection and segmentation using deep region based convolutional neural network and fuzzy C-means clustering," Int. J. Med. Inform., vol. 124, pp. 37–48, 2019, Accessed: May 27, 2020. [Online]. Available: https://www.sciencedirect.com/science/article/pii/S1386505618307470.

[17] H. Ullah et al., "An ensemble classification of exudates in color fundus images using an evolutionary algorithm based optimal features selection," Microsc. Res. Tech., vol. 82, no. 4, pp. 361–372, Apr. 2019, doi: 10.1002/jemt.23178.

[18] F. Afza, M. A. Khan, M. Sharif, and A. Rehman, "Microscopic skin laceration segmentation and classification: A framework of statistical normal distribution and optimal feature selection," Microsc. Res. Tech., vol. 82, no. 9, pp. 1471–1488, Sep. 2019, doi: 10.1002/jemt.23301.

[19] M. A. Khan, M. I. Sharif, M. Raza, A. Anjum, T. Saba, and S. A. Shad, "Skin lesion segmentation and classification: A unified framework of deep neural network features fusion and selection," Expert Syst., Dec. 2019, doi: 10.1111/exsy.12497.

[20] M. Hasan, M. Kamal, and H. Chowdhury, "Automatic Detection and Analysis of Melanoma Skin Cancer using Dermoscopy Images Network Periphery View project Machine Learning (Introduction) View project," Int. J. Recent Technol. Eng., vol. 8, no. 3, pp. 2277–3878, 2019, doi: 10.35940/ijrte.C4561.098319.

[21] L. Sánchez-Reyes, J. R.-R.-A. Sciences, and undefined 2020, "A High-Accuracy Mathematical Morphology and Multilayer Perceptron-Based Approach for Melanoma Detection," mdpi.com, vol. 10, no. 3, p. 1098, 2020, Accessed: Jul. 11, 2020. [Online]. Available: https://www.mdpi.com/2076-3417/10/3/1098.

[22] Commission Internationale de l'Éclairage, "Recommendations on uniform color spaces, color-difference equations, psychometric color terms," CIE Publ. 15 Suppl. 2Commission Int. l'Éclairage Paris, Fr., pp. 135–178, 1978.

[23] A. R. Ali, J. Li, and S. J. O'Shea, "Towards the automatic detection of skin lesion shape asymmetry, color variegation and diameter in dermoscopic images," PLoS One, vol. 15, no. 6, Jun. 2020, doi: 10.1371/journal.pone.0234352.

[24] A. B. Tajeddin NZ, "Melanoma recognition in dermoscopy images using lesion's peripheral region information," Comput. Methods Programs Biomed., vol. 163, pp. 143–153, 2018, Accessed: Jul. 12, 2020. [Online]. Available: https://www.sciencedirect.com/science/article/pii/S0169260717313251.

[25] L. Bi, J. Kim, E. Ahn, D. Feng, and M. Fulham, "Automated skin lesion segmentation via image-wise supervised learning and multi-scale superpixel based cellular automata," in Proceedings - International Symposium on Biomedical Imaging, Jun. 2016, vol. 2016-June, pp. 1059–1062, doi: 10.1109/ISBI.2016.7493448.

[26] I. Sanchez and S. Agaian, "A new system of computer-aided diagnosis of skin lesions," in Image Processing: Algorithms and Systems X; and Parallel Processing for Imaging Applications II, Feb. 2012, vol. 8295, pp. 82–95, doi: 10.1117/12.906796.

[27] A. Pennisi, D. D. Bloisi, D. Nardi, A. R. Giampetruzzi, C. Mondino, and A. Facchiano, "Melanoma detection using delaunay triangulation," in Proceedings - International Conference on Tools with Artificial Intelligence, ICTAI, Jan. 2016, pp. 791–798, doi: 10.1109/ICTAI.2015.117.

[28] A. Pennisi, D. D. Bloisi, D. Nardi, A. R. Giampetruzzi, C. Mondino, and A. Facchiano, "Skin lesion image segmentation using Delaunay Triangulation for melanoma detection," Comput. Med. Imaging Graph., vol. 52, pp. 89–103, Sep. 2016, doi: 10.1016/j.compmedimag.2016.05.002.

[29] M. Silveira et al., "Comparison of segmentation methods for melanoma diagnosis in dermoscopy images," IEEE J. Sel. Top. Signal Process., vol. 3, no. 1, pp. 35–45, 2009, doi: 10.1109/JSTSP.2008.2011119.

[30] E. Ahn et al., "Saliency-Based Lesion Segmentation Via Background Detection in Dermoscopic Images," IEEE J. Biomed. Heal. Informatics, vol. 21, no. 6, pp. 1685–1693, Nov. 2017, doi: 10.1109/JBHI.2017.2653179.

[31] H. Fan, F. Xie, Y. Li, Z. Jiang, and J. Liu, "Automatic segmentation of dermoscopy images

using saliency combined with Otsu threshold," Comput. Biol. Med., vol. 85, pp. 75–85, Jun. 2017, doi: 10.1016/j.compbiomed.2017.03.025.

[32] S. M. Jaisakthi, P. Mirunalini, and C. Aravindan, "Automated skin lesion segmentation of dermoscopic images using GrabCut and kmeans algorithms," IET Comput. Vis., vol. 12, no. 8, pp. 1088–1095, Dec. 2018, doi: 10.1049/iet-cvi.2018.5289.

[33] A. Masood and A. Al-Jumaily, "Orientation Sensitive Fuzzy C Means Based Fast Level Set Evolution for Segmentation of Histopathological Images to Detect Skin Cancer," in Advances in Intelligent Systems and Computing, Dec. 2020, vol. 923, pp. 501–510, doi: 10.1007/978-3-030-14347-3_49.

[34] N. Dey, V. Rajinikanth, A. Ashour, and J. M. Tavares, "Social Group Optimization Supported Segmentation and Evaluation of Skin Melanoma Images," Symmetry (Basel)., vol. 10, no. 2, p. 51, Feb. 2018, doi: 10.3390/sym10020051.

[35] P. M. M. Pereira et al., "Dermoscopic skin lesion image segmentation based on Local Binary Pattern Clustering: Comparative study," Biomed. Signal Process. Control, vol. 59, p. 101924, May 2020, doi: 10.1016/j.bspc.2020.101924.

[36] R. Javed, M. S. M. Rahim, T. Saba, and A. Rehman, "A comparative study of features selection for skin lesion detection from dermoscopic images," Netw. Model. Anal. Heal. Informatics Bioinforma., vol. 9, no. 4, Dec. 2020, doi: 10.1007/s13721-019-0209-1.

[37] M. Nasir, M. Attique Khan, M. Sharif, I. U. Lali, T. Saba, and T. Iqbal, "An improved strategy for skin lesion detection and classification using uniform segmentation and feature selection based approach," Microsc. Res. Tech., vol. 81, no. 6, pp. 528–543, Jun. 2018, doi: 10.1002/jemt.23009.

[38] J. Yap, W. Yolland, and P. Tschandl, "Multimodal skin lesion classification using deep learning," Exp. Dermatol., vol. 27, no. 11, pp. 1261–1267, Nov. 2018, doi: 10.1111/exd.13777.

[39] H. Mahmoud, M. Abdel-Nasser, and O. A. Omer, "Computer aided diagnosis system for skin lesions detection using texture analysis methods," in Proceedings of 2018 International Conference on Innovative Trends in Computer Engineering, ITCE 2018, Mar. 2018, vol. 2018-March, pp. 140–144, doi: 10.1109/ITCE.2018.8327948.

[40] T. Y. Tan, L. Zhang, and C. P. Lim, "Adaptive melanoma diagnosis using evolving clustering, ensemble and deep neural networks," Knowledge-Based Syst., vol. 187, p. 104807, Jan. 2020, doi: 10.1016/j.knosys.2019.06.015.

[41] D. C. Chang and W. R. Wu, "Image contrast enhancement based on a histogram transformation of local standard deviation," IEEE Trans. Med. Imaging, vol. 17, no. 4, pp. 518–531, 1998, doi: 10.1109/42.730397.

[42] V. A. Wold JH, "The derivation of XYZ tristimulus spaces: A comparison of two alternative methods," Color Res. Appl. Wiley Online Libr., vol. 26, pp. 222–224, 2001, Accessed: Aug. 09, 2020. [Online]. Available: https://onlinelibrary.wiley.com/doi/abs/10.1002/1520-6378(2001)26:1+%3C::AID-COL47%3E3.0.CO;2-4?casa_token=q7qM_oHyRQQAAAAA:SuolMHCXsKxI5Qtg3H84Jyv2XTm_C14FWchIQyQV1FDUwotjbzuCX6jjUWJNBcbUbEZh5hZOnwui2oRt.

[43] Z. Jinwei and Y. S. C. L. Y. O. Jinwei ZH, "Dark channel prior-based image dehazing with atmospheric light validation and halo elimination," J. Image Graph., vol. 21, no. 9, pp. 1221–1228, 2016, Accessed: Aug. 09, 2020. [Online]. Available: http://en.cnki.com.cn/Article_en/CJFDTotal-ZGTB201609011.htm.

[44] X. Wang, Y. Liu, Y. Chen, and Y. Liu, "An Adaptive Density-Based Time Series Clustering Algorithm: A Case Study on Rainfall Patterns," ISPRS Int. J. Geo-Information 2016, vol. 5, no. 11, p. 245, Nov. 2016, doi: 10.3390/IJGI5110205.

[45] B. Xu, N. Wang, T. Chen, and M. Li, "Empirical Evaluation of Rectified Activations in Convolutional Network," arXiv Prepr. arXiv1505.00853, May 2015, Accessed: Aug. 09, 2020. [Online]. Available: http://arxiv.org/abs/1505.00853.

[46] "ISIC Archive," The Shore Family Fund, 2016. https://www.isic-archive.com/#!/topWithHeader/wideContentTop/main (accessed Dec. 16, 2019).

[47] T. Mendonça, A. R. S. Marçal, and C. Barata, "PH2: A Public Database for the Analysis of Dermoscopic Images Automated detection and characterization of impact craters View project A dynamic analysis of the impact of climate change on the wine production in the Douro area. View project," Dermoscopy image Anal., doi: 10.1201/b19107-14.

[48] N. N. Sultana, B. Mandal, and N. B. Puhan, "Deep residual network with regularised fisher framework for detection of melanoma," IET Comput. Vis., vol. 12, no. 8, pp. 1096–1104, Dec. 2018, doi: 10.1049/iet-cvi.2018.5238.

[49] F. Xie, J. Yang, J. Liu, and Z. Jiang, "Skin lesion segmentation using high-resolution convolutional neural network," Comput. Methods Programs Biomed., pp. 105–241, 2020, Accessed: Aug. 09, 2020. [Online]. Available: https://www.sciencedirect.com/science/article/pii/S0169260719306637.